



Comparative study of dimensionality and superconducting parameters in YBCO–NaNbO₃ nanoparticles- and nanorods-added composite sample from excess conductivity analysis

Mamta Dahiya¹ · Rohit Kumar² · Dheeraj Kumar¹ · Neeraj Khare^{1,2}

Received: 16 September 2021 / Accepted: 21 January 2022 / Published online: 15 March 2022
© The Author(s), under exclusive licence to Springer-Verlag GmbH, DE part of Springer Nature 2022

Abstract

Excess conductivity and dimensional fluctuation effects on the superconducting parameters with the addition of nanoparticles (NPs) or nanorods (NRs) of NaNbO₃ in polycrystalline YBa₂Cu₃O_{7-δ} (YBCO) have been studied. Two series of samples were synthesized by solid-state reaction route on addition of 0.5 wt% to 2.0 wt% NaNbO₃ NPs or NRs in pure YBCO superconductor. X-ray diffraction results show the unaffected orthorhombic crystal structure for all the synthesized samples. The field emission scanning electron microscope and high-resolution transmission electron microscope images reflect the addition of NPs or NRs in the YBCO material and indicate that the higher wt% of additive material leads to agglomeration of NPs or NRs. Using the Aslamazov–Larkin model, the fluctuation conductivity and the superconducting parameters such as coherence lengths, critical magnetic fields ($B_{C1}(0)$ and $B_{C2}(0)$), effective layer thickness (d) and critical current densities (J_C) have been estimated. It has been observed that 0.5 wt% concentration of addition of NaNbO₃ NPs or NRs in YBCO compound shows significant enhancement in $B_{C1}(0)$, $B_{C2}(0)$ and $J_C(0)$, whereas a further increase in additive material results in a decrease in superconducting parameters. In comparison with the pure YBCO, the addition of NPs or NRs is causing a reduction in the magnetic vortex motion that leads to an enhancement in the vortex pinning capability which is responsible for increasing the $B_{C1}(0)$, $B_{C2}(0)$ and $J_C(0)$. Furthermore, a detailed analysis confirmed that the addition of NRs of NaNbO₃ in YBCO is much more effective compared to the NPs for the same wt% of additive material.

Keywords YBCO superconductor · NaNbO₃ nanoparticles · NaNbO₃ nanorods · Excess conductivity · Coherence length · Critical current density

1 Introduction

Most of the oxides-based superconductors such as YBa₂Cu₃O_{7-δ} (YBCO) and Bi₂Sr₂CaCu₂O_{8+x} (BSCCO) are among the most studied high-temperature superconductors (HTSs) due to their several interesting superconducting properties such as high critical temperature (T_C), low charge carrier concentration, anisotropic nature, granular morphology and small coherence length, which make them suitable candidate for using in various practical applications [1–3].

High values of critical current density (J_C) at high magnetic fields are desirable for using these compounds in practical applications. Low connectivity between the weak links of the grain boundaries and moderate values of J_C for YBCO at higher magnetic fields and temperatures impose limitations for their use in several applications [4–7]. Various methods have been used in previous studies to improve the superconducting properties, like chemical doping, ion irradiation and addition of the nano-entities in the superconducting materials [4, 5, 8, 9]. It has been observed that the appropriate amount, optimal density, size and type of the added nano-entities in the matrix of YBCO play a crucial role during the interaction between these entities and flux line networks. Furthermore, these nano-entities can create defects (point and columnar defects), oxygen vacancies, impurity phases and precipitate, etc., in the superconductor crystal structure which can cause a variation in the coupling strength and composition of the grain boundaries [10–13]. In addition,

✉ Neeraj Khare
nkhare@physics.iitd.ernet.in

¹ Department of Physics, Indian Institute of Technology Delhi, Hauz Khas, New Delhi, Delhi 110016, India

² Nanoscale Research Facility, Indian Institute of Technology Delhi, Hauz Khas, New Delhi, Delhi 110016, India

an excess density of these nano-entities can produce disorder in the superconducting system which can deteriorate the superconducting properties [12–14].

For YBCO superconductor, various parameters like small coherence length, anisotropy and low density of charge carriers are responsible for rounding off the resistivity curve which is correlated with the fluctuation in the order parameter of the superconducting Cooper pair in the large temperature range away from the superconducting transition [15, 16]. Existence of the Cooper pairs above the critical temperature provides finite lifetime due to the thermal fluctuations, and their creation provides an increase in the excess conductivity which is used to estimate the microscopic parameters [17, 18]. The concept of excess conductivity arises due to the discontinuous second-order phase transition occurring near the critical temperature. The excess conductivity induced due to the thermal fluctuations is used to understand the conduction mechanism in the HTS materials. The excess conductivity fluctuations measured in HTS due to anisotropic nature show structure dependence of the order parameter. Various microscopic and macroscopic parameters such as order parameter dimensionality, coherence length (along *c*-axis), crossover temperature, penetration depth, upper and lower critical magnetic field and critical current density can be estimated from the excess conductivity analysis [19, 20]. There are various models like Lawrence–Doniach (L-D) [21], Aslamazov and Larkin (A-L) [22], and Maki–Thompson (M-T) [23] to investigate the fluctuation-induced conductivity effects. A-L approach is the most convenient and easy method to extract the intrinsic superconducting parameters from the excess conductivity analysis. Recently, Hannachi et al. [13] has shown dominance of the 3D region and enhancement in the critical current density of the YBCO–TiO₂ nanowires (NWs) composite samples for 0.1 wt% added sample which reduces flux motion due to addition of TiO₂ NWs. A decrease in the value of coherence length and an enhancement in the superconducting parameters such as $B_{C1}(0)$, $B_{C2}(0)$ and $J_C(0)$ for $x = 0.05$ wt.% concentration of WO₃ nanoparticles (NPs) have been reported [24]. It has been observed that the improvement in the flux pinning ability is due to the decrease in the vortex motion in the composite samples, while on a further increase in the WO₃ content, a decrement has been observed in the superconducting properties [24]. Slimani et al. [25] have also illustrated an improvement in the $B_{C1}(0)$, $B_{C2}(0)$ and $J_C(0)$ for $x = 0.1$ wt.% concentration of WO₃ NWs inclusion compared to pure sample. Sahoo et al. [5] have reported an increment in the 2D fluctuation and decrement in 1D and 3D fluctuation regime after addition of cobalt ferrite nanoparticles of average size 58 nm. Al-Otaibi et al. [26] have illustrated a comparative study between the SiO₂ NPs and NWs composite samples and reported an improvement in the $B_{C1}(0)$, $B_{C2}(0)$ and $J_C(0)$ values with the addition of NPs

in comparison with NWs-added samples. There have been various studies on NPs and NWs-added YBCO composite samples, but few reports on their comparative study have been performed earlier. The purpose of choosing NaNbO₃ in the present study as a nano-additive in YBCO is due to its perovskite's crystal structure. NaNbO₃ material has an orthorhombic crystal structure at room temperature [27, 28]. We have used NaNbO₃ powder in two different morphologies, viz. nanoparticles and nanorods. The main objective of the present work is to analyze the effect of addition of NPs or NRs on the superconducting properties of YBCO and thereby deduce its effect on superconducting properties such as coherence length, penetration depth, $B_{C1}(0)$, $B_{C2}(0)$ and $J_C(0)$.

In the present work, we have carried out a comparative study of the impact of NaNbO₃ NPs or NRs on the fluctuation-induced conductivity above the critical temperature in the pure YBCO and nanocomposite samples. AL and LD model has been used to perform the excess conductivity analysis to calculate the crossover temperatures and various fluctuation regimes. The dimensionality and various superconducting parameters like $B_{C1}(0)$, $B_{C2}(0)$, $J_C(0)$ and coherence length along *c*-axis have been calculated, and the mechanism of conduction has been discussed, in order to study the impact of NPs or NRs on pure YBCO.

2 Experimental details

2.1 Synthesis methods

2.1.1 Synthesis of NaNbO₃ nanoparticles

Hydrothermal method was used to synthesize sodium niobate nanoparticles. Firstly, a 3 M of sodium hydroxide (NaOH) (99.99%) was dispersed in 80 ml of deionized water with vigorous stirring for 30 min. Afterward, 30 mM of niobium pentoxide (Nb₂O₅) (99.99%) was put into the above mixture and stirred for 2 h. The above aqueous solution was transferred to the 100 ml Teflon-lined stainless steel autoclave and put into a hot air oven at 150 °C for 24 h. Finally, the product was washed with deionized water several times and dried at 70 °C for 24 h.

2.1.2 Synthesis of NaNbO₃ nanorods

Sodium niobate nanorods were synthesized using a hydrothermal method. Nb₂O₅ (99.99%) and NaOH (99.99%) were used as a starting precursor. For the typical procedure, 60 mM of Nb₂O₅ was dispersed in 50 ml of deionized water and stirred for 30 min. Afterward, 12 M of NaOH was mixed in the above aqueous solution with vigorous stirring for 2 h. The solution was transferred to a Teflon-lined stainless steel

autoclave and was kept into a hot air oven and heated at 160 °C for 4 h. The resultant product was washed several times with deionized water and dried at 70 °C for 24 h. Finally, the product was heat-treated at 550 °C for 6 h.

2.1.3 Synthesis of pure YBCO and nanocomposite samples

Pure YBCO and nanocomposite samples were synthesized by the standard solid-state reaction method. The precursors used were of high-purity powders of Y₂O₃ (99.99%), BaCO₃ (99.99%) and CuO (99.99%), respectively. The precursors used were mixed according to the stoichiometric ratio of Y:Ba:Cu = 1:2:3 and grinded thoroughly for 3–4 h. The grinded powder was placed in alumina boat for calcination in the tubular furnace at 900 °C for 12 h, and this step was repeated two more times with intermediate grinding to get homogenous powder of YBCO. The calcined powder was regrinded and pressed in a pellet using hydraulic machine with a pressure of 2500 psi. The pellet was kept in the furnace for sintering at the temperature of 930 °C for 12 h under oxygen atmosphere with an intermediate annealing at 600 °C for 8 h. For synthesizing nanocomposite samples, NaNbO₃ powder in the form of NPs or NRs was added with 0.5, 1.0 and 2.0 wt% concentration in the calcined YBCO powder and then grinded and pelletized. Afterward, the pellets were sintered using the heating and cooling rate similar to the one used for the synthesis of pure YBCO.

2.2 Characterization

The confirmation of phase formation for the pure and nanocomposite samples was done by X-ray diffractometer (XRD) with Rigaku Ultima IV diffractometer instrument

equipped with Ni-filtered using CuK_α radiation source with wavelength, $\lambda = 1.54 \text{ \AA}$. The surface morphology analysis was performed by using field emission scanning electron microscope (FESEM) with Oxford energy-dispersive X-ray (EDX) spectroscopy system (Model no. FEI Quanta 200 FESEM). High-resolution transmission electron microscopy (HRTEM) studies were conducted using FEI Tecnai transmission electron microscope. Four-probe method was used to perform the transport measurement to observe the resistivity variation with temperature by using Lakeshore temperature controller (model no. 325), Keithley Nanovoltmeter (model no. 2182A), Keithley DC and AC current source (model no. 6221) and liquid helium cryostat.

3 Results and discussion

3.1 XRD analysis

The confirmation for phase formation was carried out from XRD spectra for the pure and composite samples as shown in Fig. 1. The XRD diffraction spectra of pure YBCO were matched with the standard spectra and found to be in good agreement with JCPDS file 89–5732, which confirms the orthorhombic phase formation, whereas in the XRD spectrum of the NaNbO₃ nanostructure, i.e., NPs or NRs, the peaks are in good correlation with JCPDS data 82–0606, which has confirmed the orthorhombic phase of NaNbO₃. In addition, the XRD spectra of composite samples have shown neither any kind of peak shifting nor extra peak corresponding to any other phase formation which indicates that the crystal structure of YBCO in the YBCO–NaNbO₃ nanocomposites remains unchanged, while no other peaks

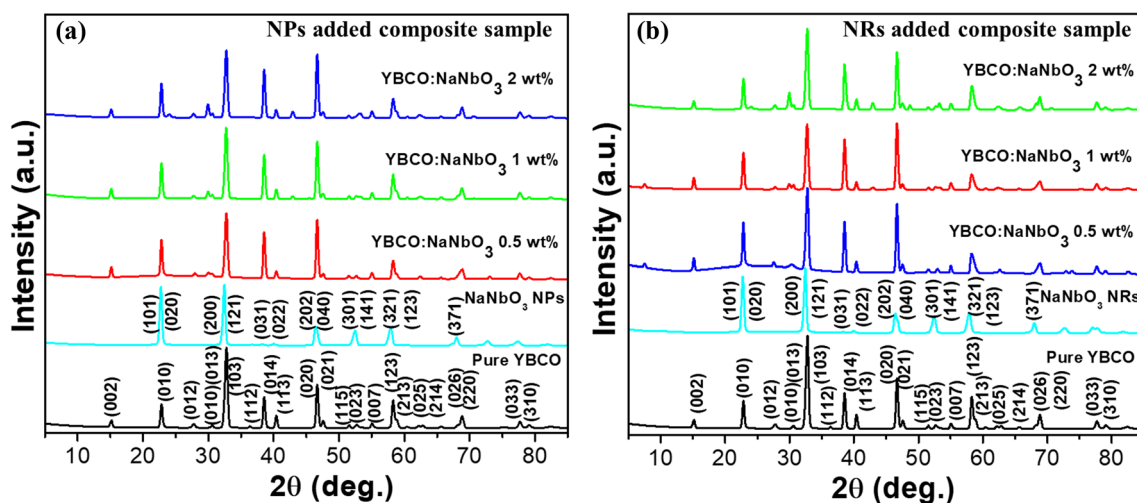


Fig. 1 XRD spectra of the **a** pure YBCO, NaNbO₃ NPs, YBCO–*x*NaNbO₃ NPs nanocomposite samples, and **b** pure YBCO, NaNbO₃ NRs, YBCO–*x*NaNbO₃ NRs nanocomposite samples with *x* = 0.5, 1.0, 2.0 wt% concentrations

were observed in the XRD spectra because most of the peaks of NaNbO_3 were observed at the same 2θ position as in pure YBCO sample.

3.2 Morphology and microstructure analysis

FESEM pictures of the nanorods (NRs) and nanoparticles (NPs) are depicted in Fig. 2a and b, respectively, for estimating the dimension of the added NRs or NPs. The length of these nanorods is in the range from 0.5 to 2 μm , whereas its diameter is in the range of 100–150 nm. The nanoparticles of NaNbO_3 have spherical shapes with diameter as 100–200 nm.

The morphology, size, and shape of the microstructure in the pure and nanocomposite samples were analyzed by FESEM and HRTEM techniques, and the images are shown in Figs. 3 and 4, respectively. Randomly oriented grains of different shapes and sizes in pure YBCO were observed in FESEM images as shown in Fig. 3, while in the nanocomposite samples, NRs and NPs were observed on the surface and between the grain boundaries among the pore spaces of YBCO compound. The presence of NPs or NRs between the grains of YBCO may be useful to improve the pinning properties in the YBCO– NaNbO_3 nanocomposite samples. Increasing concentration of NPs or NRs in the composite samples leads to the denser and compact packing of grains along with the agglomeration of NPs or NRs on the surface.

In HRTEM images (Fig. 4), the lattice fringes were clear with inter-planar spacing of 0.24 nm which corresponds to the plane (103). In the 2 wt% NRs and NPs NaNbO_3 -added YBCO composite samples, the lattice fringes were being observed with inter-planar spacing of 0.24 nm corresponding to (103) plane of YBCO and the inter-planar spacing of 0.34 nm corresponding to (020) plane of NaNbO_3 . It can be concluded from HRTEM study that NPs and NRs are present in the matrix of YBCO compound and hence are expected to improve the pinning properties.

3.3 Electrical resistivity curve analysis

Figure 5 presents the variation of resistivity (ρ) with temperature for the pure YBCO and nanocomposite samples. The plot of resistivity curve is exhibiting two types of variations: (i) nonlinear behavior near the superconducting transition region and (ii) linear behavior in the normal metallic state which is expressed by the Anderson and Zou formula [29]:

$$\rho(T) = \rho_0 + \alpha T \quad (1)$$

where $\rho(T)$ is the normal state resistivity which depends on the porosity, inter- and intra-grain properties of the sample, α is the slope, $\left(\frac{d\rho}{dT}\right)$ is calculated from the linear fitting of the resistivity curve and ρ_0 is the intercept obtained from extrapolating the linearly fitted data to 0 K which is equivalent to the residual resistivity and independent of temperature but influenced by the presence of impurity, defects density and heterogeneity [24, 25]. Table 1 shows the value of T_C , T_{CO} , T_{CO}^{onset} , ρ_{300} and ρ_0 for YBCO and nanocomposite samples. T_{CO}^{onset} is the temperature where the resistivity starts decreasing, and T_{CO} is the temperature where the resistivity becomes zero. T_C is the temperature corresponding to the maximum value of $\frac{d\rho}{dT}$ in the plot of $\frac{d\rho}{dT}$ versus T curve.

Figure 6a depicts the variation of ρ_{300} and ρ_0 with the x wt% ($x = 0.5, 1.0$ and 2.0 wt%) of NaNbO_3 NPs or NRs added in YBCO– $x\text{NaNbO}_3$ nanocomposite samples. The values of ρ_{300} and ρ_0 are observed to decrease after 0.5 wt% addition of NRs or NPs of NaNbO_3 in YBCO samples. After a further increase in the addition of NRs or NPs, the value of ρ_{300} and ρ_0 shows an increment. The increase in resistivity of YBCO nanocomposite samples can be attributed to enhanced disorder and heterogeneity after adding NPs or NRs in YBCO samples. The value of T_C for NPs-added YBCO composite sample shows an increase of 0.5 wt% addition, whereas it decreases as the added percentage is increased. However, for the NRs-added YBCO, it has been observed that T_C shows a decrease with addition of more

Fig. 2 FESEM images of the synthesized **a** NaNbO_3 NRs, and **b** NaNbO_3 NPs

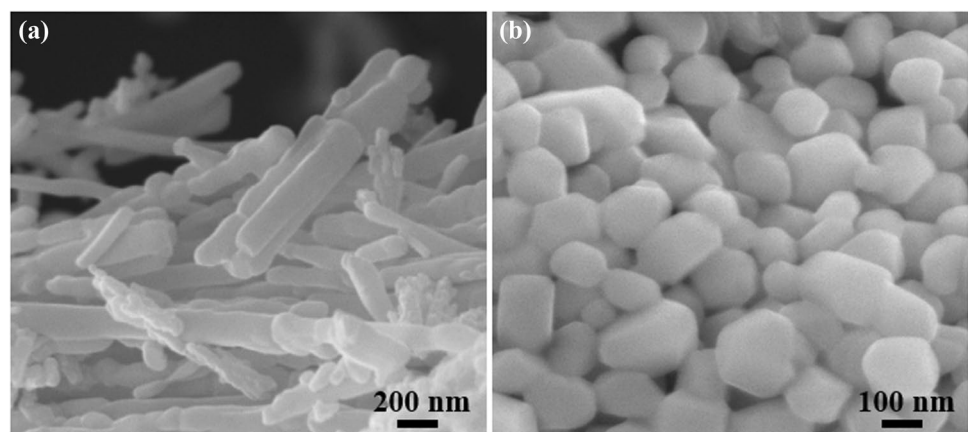
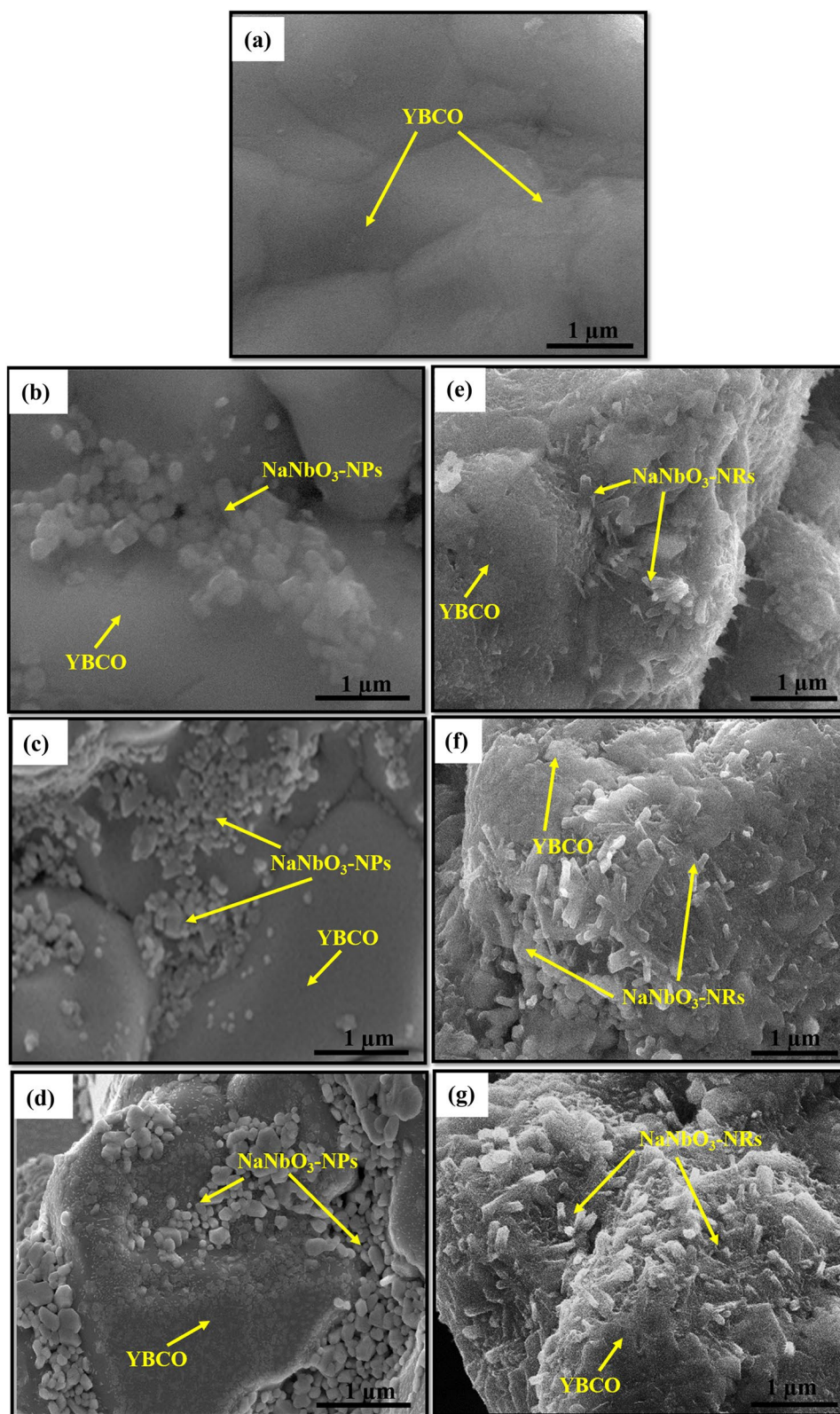


Fig. 3 FESEM images of the **a** pure YBCO, **b** 0.5, **c** 1.0, **d** 2.0 wt% NPs-added and **e** 0.5, **f** 1.0, **g** 2.0 wt% NRs-added YBCO–*x*NaNbO₃ nanocomposite samples



percentage of NRs of NaNbO₃. The change in the value of T_C is mainly attributed to the increase in disorder and modification in the grain boundary characteristic with additions

of NPs or NRs in the nanocomposite samples, which is in the good correlation with the FESEM images. The addition of higher percentage of NaNbO₃ in YBCO resulted in the

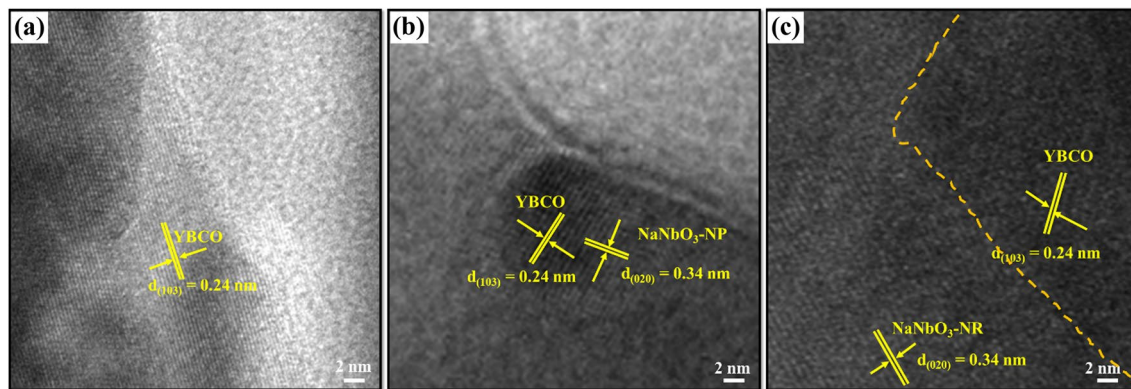


Fig. 4 HRTEM images of the a pure YBCO and, b 2 wt% NPs-added, c 2 wt% NRs-added YBCO–NaNbO₃ nanocomposite samples

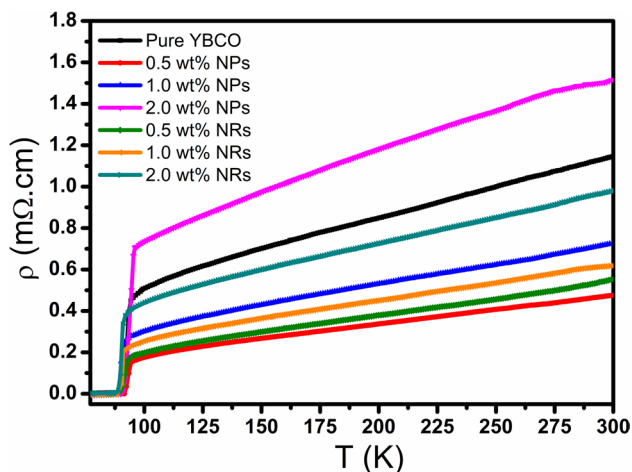


Fig. 5 Electrical resistivity versus temperature dependence curve of pure YBCO and YBCO–xNaNbO₃ with x=0.5, 1.0, and 2.0 wt% NPs- or NRs-added nanocomposite samples

Table 1 Characteristics parameters deduced from the resistivity vs temperature curve for YBCO + xNaNbO₃ nanocomposite

x wt% concentration	$T_{CO} \pm 1$ (K)	$T_C \pm 1$ (K)	α (mΩ-cm.K ⁻¹)	p
0.0	90.74	91.69	0.0029	0.146
0.5 wt% NPs	92.19	93.05	0.0013	0.160
1.0 wt% NPs	91.43	93.12	0.0019	0.150
2.0 wt% NPs	91.17	93.61	0.0040	0.148
0.0	90.74	91.69	0.0029	0.160
0.5 wt% NRs	90.60	91.84	0.0015	0.156
1.0 wt% NRs	90.10	90.65	0.0017	0.151
2.0 wt% NRs	89.44	90.27	0.0025	0.147

(NPs—nanoparticles; NRs—nanorods)

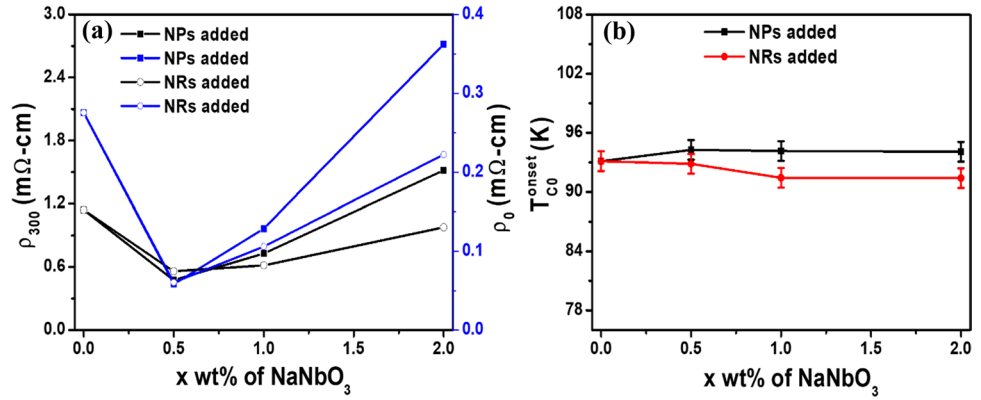
excess disorders and agglomeration which tends to affect the superconducting transition temperature by decreasing both the T_{CO} and T_{CO}^{onset} (as shown in Fig. 6b) as compared to the pure sample [25].

The broad width of the transition region was an indicator of change in the intergranular properties. T_{CO}^{On} is affected by concentration of the hole carriers (p) in the YBCO matrix which can be estimated by using the following formula [30]:

$$p = 0.16 - \left[\frac{\left(1 - \frac{T_{CO}}{T_{CO}^{max}}\right)^{0.5}}{82.6} \right] \tag{2}$$

where T_{CO}^{max} is the relative maximum value of T_{CO} among the pure and composite sample. Table 1 also shows the value of p for YBCO and all nanocomposite samples. The maximum value of T_{CO} was 90.74 K for pure and NRs-added samples, and hence, the value of p was calculated according to this value. For NRs-added samples, the value of $p = 0.16$ was maximum for pure YBCO, and with the increase in the concentration of NRs in the composite samples, the value of T_{CO} starts decreasing which was representing a decrement in the hole carrier concentration in the CuO₂ planes with the increase in the concentration of NRs, while in the case of NPs-added samples, it was observed that with an increase in the value of NPs concentration, the value of T_{CO} first increases and then decreases with the increase in the concentration of NPs. The value of $T_{CO}^{max} = 92.19$ K was for the 0.5 wt% NPs-added sample among the pure and NPs-added samples. The value of p for the 0.5 wt% NPs and pure sample was 0.160 and 0.146, respectively, which indicates an increase in the hole carrier concentration in 0.5 wt% NPs-added sample as compared to the pure sample, while a decrease in the value of p was observed with a further increase in the NPs concentration in the composite samples.

Fig. 6 Variation of **a** ρ_{300} and ρ_0 , and **b** T_{CO}^{onset} with the x wt% of NaNbO₃ NPs or NRs added in YBCO– x NaNbO₃ nanocomposite samples with $x=0.5, 1.0$ and 2.0 wt%



The increase in ρ_{300} value for 2.0 wt% NPs-added composite sample as compared to pure sample can be attributed to low hole charge carrier concentration in CuO₂ plane and also due to more agglomeration of NPs on the surface of YBCO grain which was reducing the coupling strength of superconducting grains by creating weak links, and these were modifying the intergranular links properties by converting them from non-dissipative to dissipative state, hence decreasing the value of T_C .

3.4 Excess conductivity

Excess conductivity for high-temperature superconductors (HTS) was studied by Aslamazov–Larkin (A-L) theory and Lawrence–Doniach (L-D) model in the mean field region or Ginzburg–Landau (G-L) region where the thermodynamic fluctuation appears [22, 31, 32]. Such thermal fluctuations lead to the formation of Cooper pairs above the superconducting transition region. In the high-temperature cuprates-based superconductors, high anisotropy and short coherence length are responsible for the thermally induced conductivity [33]. The dimensionality of such fluctuation is affected by the nature of grain size, grain boundary junctions and carrier concentration in the conducting CuO₂ planes [33]. According to the AL theory, the excess conductivity diverges as [22, 32]:

$$\Delta\sigma = A\varepsilon^{-\lambda} \tag{3}$$

where $\varepsilon = \left(\frac{T}{T_C} - 1\right)$ is the reduced temperature and $\lambda = \left(2 - \frac{D}{2}\right)$, D is the dimensionality. λ is the Gaussian critical exponent that describes the conduction dimensionality of the system in the mean field regime, and the values can be determined by the slope of linear fit from the experimentally observed curve between excess conductivity versus reduced temperature [13]. The effective values of λ for three-dimensional (3D), two-dimensional (2D) and one-dimensional (1D) regimes are 0.5, 1 and 1.5, respectively [13], whereas the λ values for critical regime (CR) and shortwave

fluctuation regimes (SWF) are 0.33 and 3, respectively [24]. The constant ‘A’ is an independent parameter which could be obtained using Eq. (3). The constant ‘A’ for different regimes can also be expressed as [34]:

$$A_{3D} = \frac{e^2}{32\hbar\xi_C(0)}, \text{ for 3D fluctuation regime} \tag{4}$$

$$A_{2D} = \frac{e^2}{16\hbar d}, \text{ for 2D fluctuation regime} \tag{5}$$

$$A_{1D} = \frac{e^2\xi_C(0)}{32\hbar s}, \text{ for 1D fluctuation regime} \tag{6}$$

Here, $\xi_C(0)$ is the coherence length along c-axis, ‘e’ is the electronic charge, $\hbar = \frac{h}{2\pi}$, h is the Planck’s constant, ‘d’ is the effective conduction layer thickness in the 2D regime and ‘s’ is the cross-sectional area of conducting strips which is responsible for the conduction of charge carrier in 1D regime.

Also, $\Delta\sigma$ is defined as [34]:

$$\Delta\sigma = \frac{1}{\rho(T)} - \frac{1}{\rho_n(T)} = \sigma(T) - \sigma_n(T) \tag{7}$$

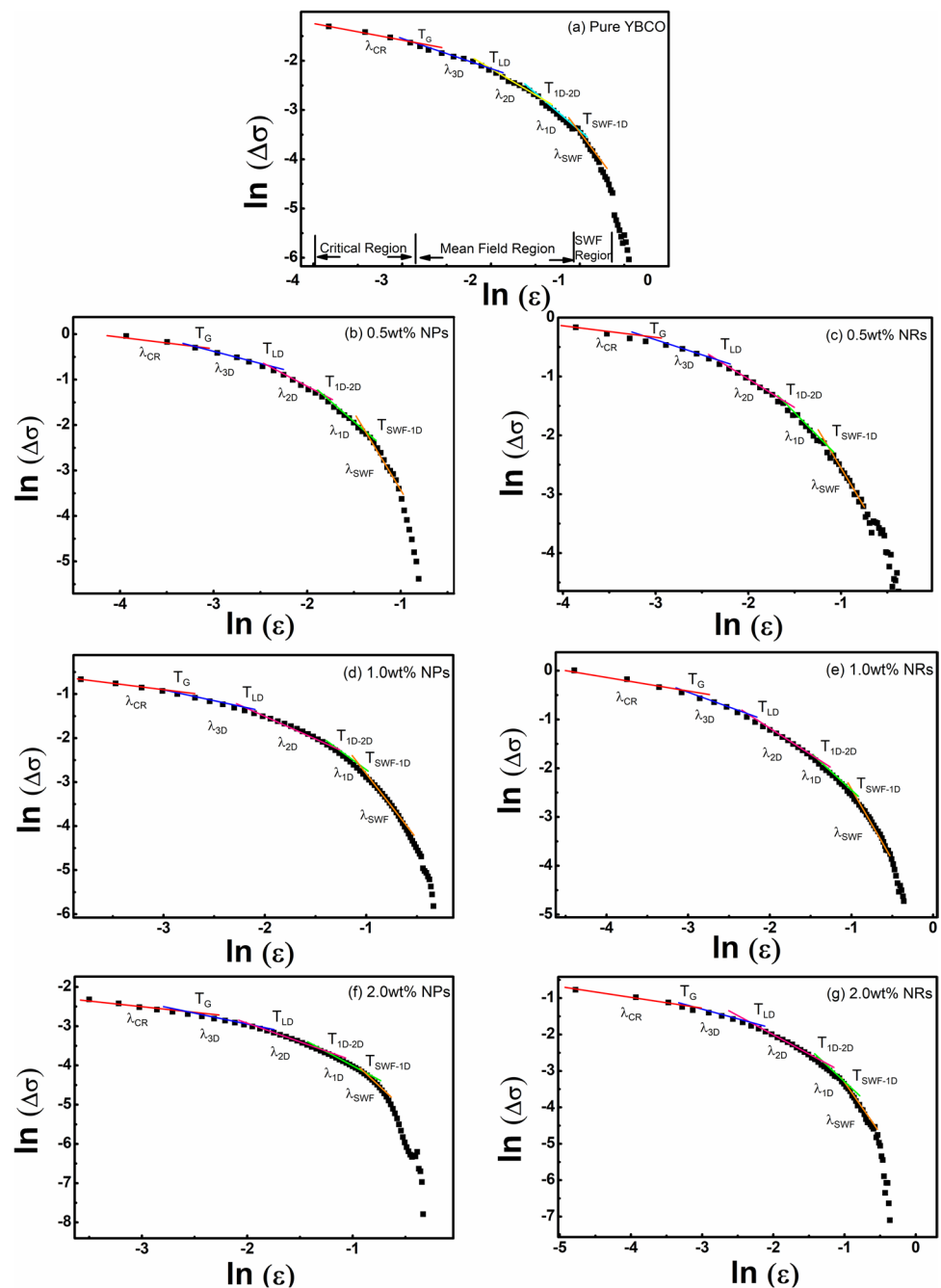
where $\rho(T)$ is the measured resistivity and $\rho_n(T)$ is the extrapolated resistivity. In our calculation, we have taken the temperature range of 150 K to 225 K for the determination of $\rho_n(T)$. The crossover temperature T_{LD} showing the transition from 2D to 3D state can be expressed as [24]:

$$T_{LD} = T_C[1 + E_J] \tag{8}$$

where E_J is the Josephson coupling constant and it can be expressed as $E_J = \left(\frac{2\xi_C(0)}{d}\right)^2$.

Figure 7 shows the $\ln(\Delta\sigma)$ versus $\ln(\varepsilon)$ plots for pure YBCO, NPs- or NRs-added YBCO–NaNbO₃ nanocomposite samples, and the fitted regions are shown by the colored lines. Each plot can be divided into three main regimes, namely the SWF regime, mean field regime and

Fig. 7 Logarithmic plot of the dependence of excess conductivity $\Delta\sigma$ on the reduced temperature ϵ for **a** pure YBCO, **b** 0.5, **c** 1.0, **d** 2.0 wt% NPs-added and **e** 0.5, **f** 1.0, **g** 2.0 wt% NRs-added YBCO- x NaNbO₃ nanocomposite samples



critical fluctuation regime [5]. The mean field regime is broadly classified into three distinctive regimes, i.e., 1D, 2D and 3D regimes. The fitted values of the critical exponents for SWF region, 1D region, 2D region, 3D region and critical regions are represented by λ_{SWF} , $\lambda_{1\text{D}}$, $\lambda_{2\text{D}}$, $\lambda_{3\text{D}}$ and λ_{CR} , respectively. Also, the crossover temperatures from SWF to 1D region, 1D to 2D region, 2D to 3D region and 3D to critical regions are represented by $T_{\text{SWF-1D}}$, $T_{1\text{D-2D}}$, T_{LD} and T_{g} , respectively, as depicted in Fig. 8 for YBCO- x NaNbO₃ NPs- or NRs-added nanocomposite samples. For all the synthesized samples, the fitted

values of critical exponents from the curves are shown in Fig. 7 and are given in Table 2.

In much higher-temperature region above $T_{\text{CO}}^{\text{onset}}$ ($T > T_{\text{CO}}^{\text{onset}}$), SWF dominates when the characteristic wavelength of the order parameter becomes the order of coherence length. Such behavior is mainly due to the change in the carrier concentration in this region that causes a change in the order parameter [33, 35]. For all the studied samples, the critical exponent values for the pure and NPs- and NRs-added YBCO samples are close to 3, which confirms the presence of SWF regime [24]. SWF regime width is mainly

associated with the oxygen vacancies in CuO₂ layer or CuO chains. Furthermore, the crossover temperature T_{SWF-1D} shows a shifting of transition from SWF regime to the mean field regime as evident from Fig. 7. Moreover, the transition boundary of mean field region and critical region is governed by the Ginzburg temperature (T_g). In the critical fluctuation region, the creation and destruction of Cooper pair is rapid [32]. The observed λ_{CR} values are in the range of 0.31–0.35, indicated the dynamical critical fluctuations, and the corresponding crossover temperatures are depicted in Table 2.

The transition width for 1D, 2D and 3D regimes is represented by $\Delta T(1D)$, $\Delta T(2D)$ and $\Delta T(3D)$, respectively, and is shown in Table 3. In HTS, the 1D crystal structure

feature does not exist, whereas the excess conductivity in 1D regime is governed by the 1D conduction channel. This conduction channel consists of a layered structure in which the high-conductivity planes of CuO₂ are well separated by the low-conductivity planes, and in this region the excess conductivity is governed by the behavior of these conduction planes. Moreover, in this regime the conduction is possible through the charge strips with cross-sectional area ‘s.’ The 1D regime shows temperature range in between the intersection of T_{SWF-1D} and T_{1D-2D} . The obtained λ_{1D} values for all the synthesized samples confirm the presence of 1D fluctuations as shown in Table 2. The transition width of 1D region, i.e., $\Delta T(1D)$, shows modification both in NPs- and in NRs-added YBCO samples as compared to the pure

Fig. 8 Variation of various crossover temperatures (T_g , T_{LD} , T_{1D-2D} and T_{SWF-1D}) with x wt% of NaNbO₃ a NPs and b NRs added in YBCO–xNaNbO₃ nanocomposite samples with x = 0.5, 1.0, and 2.0 wt%, respectively

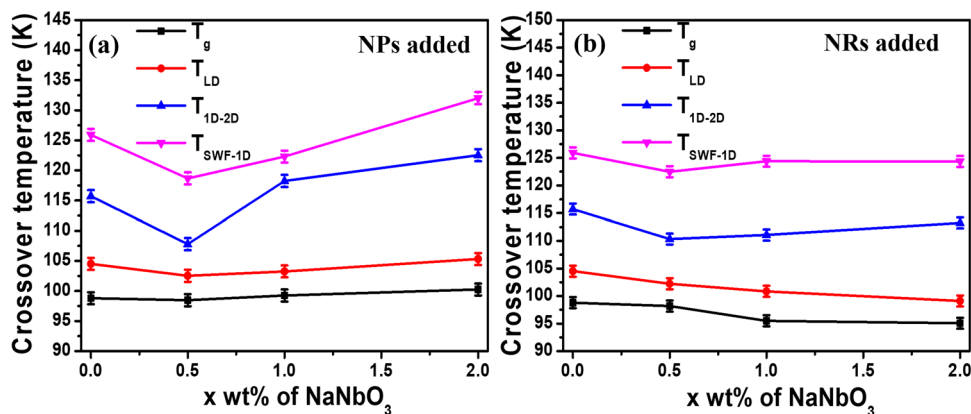


Table 2 Parameters deduced from the different fluctuation regimes such as conduction exponent from the excess conductivity analysis for YBCO + xNaNbO₃ nanocomposite

x wt% concentration	λ_{CR}	λ_{3D}	λ_{2D}	λ_{1D}	λ_{SWF}
0.0	0.35 ± 0.03	0.49 ± 0.02	0.96 ± 0.01	1.54 ± 0.04	3.03 ± 0.12
0.5 wt% NPs	0.34 ± 0.03	0.52 ± 0.03	1.00 ± 0.06	1.52 ± 0.05	3.09 ± 0.14
1.0 wt% NPs	0.33 ± 0.01	0.52 ± 0.01	0.96 ± 0.03	1.58 ± 0.08	2.99 ± 0.46
2.0 wt% NPs	0.32 ± 0.03	0.49 ± 0.01	1.00 ± 0.02	1.48 ± 0.03	3.05 ± 0.11
0.5 wt% NRs	0.31 ± 0.04	0.50 ± 0.04	0.98 ± 0.03	1.59 ± 0.09	2.95 ± 0.11
1.0 wt% NRs	0.34 ± 0.02	0.53 ± 0.02	1.00 ± 0.01	1.47 ± 0.02	3.04 ± 0.10
2.0 wt% NRs	0.32 ± 0.03	0.50 ± 0.01	1.00 ± 0.02	1.52 ± 0.04	3.01 ± 0.00

(NPs—nanoparticles; NRs—nanorods)

Table 3 Parameters derived from the excess conductivity analysis such as fluctuation region width and various other parameters for YBCO + xNaNbO₃ nanocomposite

x wt% concentration	d (nm)	s (nm ²)	$N_G (\times 10^{-2})$	$\Delta T(3D)$ (K)	$\Delta T(2D)$ (K)	$\Delta T(1D)$ (K)
0.0	9.45	19.90	7.75	5.71	11.21	10.18
0.5 wt% NPs	3.69	2.82	5.30	4.07	5.26	10.88
1.0 wt% NPs	4.83	5.47	6.59	4.0	14.98	4.05
2.0 wt% NPs	20.91	19.02	7.09	5.06	17.23	9.48
0.5 wt% NRs	3.16	2.22	6.89	4.06	8.11	12.15
1.0 wt% NRs	3.80	2.46	5.35	5.35	10.21	13.34
2.0 wt% NRs	8.72	13.07	5.32	4.05	14.13	11.13

(NPs—nanoparticles; NRs—nanorods)

sample due to the presence of high number of charge strips [5]. Furthermore, the transition width for the 1D region is also affected by the influence of elastic distortion and microscopic inhomogeneity caused by the addition of NPs or NRs which could be responsible for destabilizing the conducting charge strips. Comparing the results for the pure sample, the 1D width in NPs-added YBCO samples shows a decrease, while the NRs-added YBCO shows a significant increase, which clearly indicates that the destabilization of conducting charge strips in NPs-added samples is higher in comparison with NRs-added YBCO.

The 2D regime is represented in between the transition temperature T_{1D-2D} and T_{LD} as shown in Fig. 7. In this regime, the charge carrier conduction is possible through the conducting layer of thickness ‘d,’ where the thermal fluctuations are not high. The critical exponent in this region is close to 1 as shown in Table 2, which is in accordance with the theoretical predictions [26]. Also, the transition for $T_g < T < T_{LD}$ shows the thermal fluctuations in the 3D region where the thermal fluctuations are very high that causes charge carriers to move among the CuO_2 plane. An increase in the T_{LD} value for NPs-added samples (as shown in Fig. 8a) with higher concentration indicates the dominance of the 3D regime, while the NRs-added samples (as shown in Fig. 8b) show shift toward lower temperatures with increasing concentration of NRs, indicating the dominance of the 2D regime. It is clearly observed from Table 3 that $\Delta T(3D)$ values are decreasing compared to the respective $\Delta T(2D)$ for the same sample. The difference in the $\Delta T(3D)$ and $\Delta T(2D)$ regions is more evident in the samples with the addition of higher concentration of NRs or NPs, which in turn suggests that the grains are influenced with increasing concentration of additive nano-entities, and it can also be clearly observed from the results of FESEM images. The transition from 2D to 3D depends on the content of the added nano-entities, and also if the added nano-entities resides at the grain boundaries, it influences the superconducting transition tailing without having any significant change in the mean field region.

In the mean field region, the shifting from 3D region to 2D region toward the lower temperature is governed by the increase in the magnetic vortex motion by a reduction in the pinning capability in the system through the weak pinning source [36]. However, the increase in 2D region width specially for the higher concentration of additive material suggests that the charge carrier motion in the 2D region is very smooth which could possibly be due to the weak pinning in the system. Comparing the addition of NRs or NPs mainly for the higher concentration, the results for NPs-added samples show higher $\Delta T(2D)$ which in turn suggests that the pinning capability for NPs is weak as compared to NRs. This result is also consistent with the results of 1D region where the $\Delta T(1D)$ is higher and at close temperature range

for NRs-added YBCO composite samples as compared to NPs-added YBCO composite samples that confirms the existence of the conduction charge strips [24]. In the mean field regions, the crossover temperatures T_g , T_{LD} and T_{1D-2D} (as shown in Fig. 8) get influenced by the combined effect of added concentration of NPs or NRs, their pinning capability in YBCO matrix and accumulation on the surface of YBCO grains that causes modification in the dimensionality which is reflected in the transport properties of synthesized samples. The critical exponent in all the three regions shows good resemblance with the similar studies for YBCO superconductors [13, 24].

The crossover of 3D region to critical region associated with the relation between Ginzburg number (N_G) and the thermodynamic critical field ($B_C(0)$) under the assumptions of GL theory is expressed as [34]:

$$N_G = \left| \frac{T_g}{T_c} - 1 \right| = \frac{1}{2} \left[\frac{k_B}{B_C^2(0)\gamma^2\xi_C^3(0)} \right]^2 \quad (9)$$

Here, k_B is the Boltzmann constant and γ is the anisotropy constant.

The value of $B_C(0)$ is calculated by using Eq. (9). The value of penetration depth $\lambda_{pd}(0)$ is calculated by using the following formula [24]:

$$B_C(0) = \frac{\phi_0}{\pi\sqrt{8}\xi_C(0)\lambda_{pd}(0)} \quad (10)$$

where ϕ_0 is the flux quantum number.

The values of various thermodynamic parameters such as lower critical magnetic field ($B_{C1}(0)$), upper critical magnetic field ($B_{C2}(0)$) and critical current density ($J_C(0)$) have been estimated using the following relations [13, 34]:

$$B_{C1}(0) = \frac{\ln \kappa}{\sqrt{2}\kappa} B_C(0) \quad (11)$$

$$B_{C2}(0) = \sqrt{2}\kappa B_C(0) \quad (12)$$

$$J_C(0) = \frac{\phi_0}{3\pi\sqrt{3}\xi_C(0)\lambda_{pd}(0)^2} \quad (13)$$

where $\kappa = \lambda_{pd}/\xi$ is the GL parameter.

Using these relations, the superconducting parameters such as $\xi_C(0)$, $B_C(0)$, $B_{C1}(0)$, $B_{C2}(0)$, $J_C(0)$, and κ have been calculated and are given in Table 4. A significant change in the superconducting parameters was observed both in the NPs- and in the NRs-added composite samples, with respect to the pure YBCO sample. The observed value of coherence length for the pure YBCO samples is 1.72 nm, and on addition of NPs or NRs with 0.5 wt% concentration,

Table 4 Microscopic and macroscopic parameters such as coherence length, penetration depth, upper and lower critical magnetic field, and critical current density deduced from fluctuation-induced excess conductivity analysis for YBCO + xNaNbO₃ nanocomposite

x wt% concentration	$\xi_c(0)$ (nm)	λ (nm)	k	$B_C(0)$ (T)	$B_{C1}(0)$ (T)	$B_{C2}(0)$ (T)	$J_C(0) \times 10^5$ (A/cm ²)
0.0	1.72	8.10	4.76	16.85	3.90	111.67	2.95
0.5 wt% NPs	0.54	4.26	7.76	101.03	18.86	1190.1	11.01
1.0 wt% NPs	0.77	5.18	6.65	57.68	11.61	543.21	6.05
2.0 wt% NPs	3.92	12.05	3.07	4.92	1.27	21.29	0.22
0.5 wt% NRs	0.51	4.30	8.44	105.87	18.90	1264.4	13.3
1.0 wt% NRs	0.61	4.42	7.24	86.05	16.63	881.12	10.6
2.0 wt% NRs	1.34	6.54	4.84	26.33	6.06	180.48	2.18

(NPs—nanoparticles; NRs—nanorods)

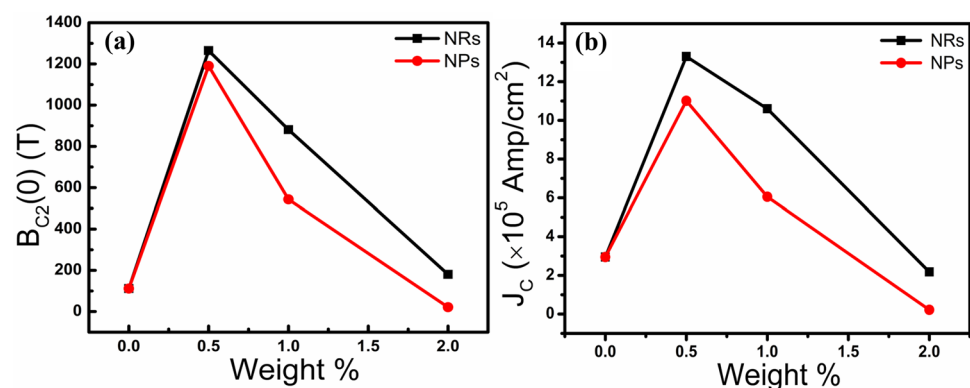
the coherence length shows drastic decrement that implies an increase in the charge carrier density in the conducting planes [24]. With the increase in the concentration level of additive material, the coherence length shows an increase which is due to the enhancement in the interlayer coupling strength. In 1D and 2D regions, the interlayer coupling sources are the charge strips with cross-sectional area ‘s’ and the conducting layers with the thickness ‘d,’ respectively, that also show significant enhancement with an increase in concentration. The reduction in the value of d for NRs-added YBCO composite sample in comparison with pure sample can be attributed to the better connectivity of grains, while in NPs-added YBCO composite sample, an increase in the value of 2 wt% NPs-added composite sample shows excess disorder and weak connectivity between the superconducting grains.

As compared to the pristine YBCO material, the NPs- or NRs-added samples show enhancement in $B_{C1}(0)$, $B_{C2}(0)$ and $J_C(0)$ values and suggest the reduction in the magnetic vortex motion while enhancement in the pinning capability. Furthermore, it is observed that these values show a continuous decrease on increasing concentration of NaNbO₃ NRs or NPs, which is possibly due to the increased defects in the samples [5]. Figure 9 shows the variation of $J_C(0)$ and $B_{C2}(0)$ with added percentage of NRs or NPs of NaNbO₃ in YBCO composite samples. In NPs-added composite sample, as the

size of the nanoparticles is greater than the coherence length, it can be considered as 3D artificial pinning centers (APCs) and NRs can be considered as the 2D APCs [36–38]. For 0.5 wt% concentration of NPs or NRs, the enhancement in the value of $J_C(0)$ of NRs is more as compared to the pure YBCO and NPs-added composite samples which may be due to creation of enough number of defect centers in the matrix of YBCO due to the presence of NaNbO₃ NRs which are acting as efficient pinning centers. However, in 1.0 wt% concentration samples, the number of defect centers has increased as compared to the 0.5 wt%, but the reduction in the $J_C(0)$ can be due to increased agglomeration of the NPs or NRs. NPs have more chances of agglomeration on surface and between grains which can be observed in FESEM images also, so their distribution is more random as their orientation can be between the vortices, along a vortex and hence acting as less efficient or weak pinning centers, whereas NRs are appearing to be more effective and strong APCs due to their two-dimensional structure.

4 Conclusion

In the present work, we have carried out a comparative study to analyze the impact of addition of NPs or NRs of NaNbO₃ on the excess conductivity analysis in the

Fig. 9 Variation of **a** upper critical magnetic field and **b** critical current density with added wt% of NPs or NRs of NaNbO₃ in the YBCO nanocomposite samples

composite samples as compared to the pure YBCO. It has been observed that the orthorhombic crystal structure of YBCO remains unchanged even after the addition of 0.5–2.0 wt% NPs or NRs of NaNbO_3 . FESEM images have shown the distribution of NPs or NRs on the surface and between the grain boundaries of YBCO. The presence of cross-fringes in the HRTEM images for NPs- or NRs-added YBCO composite samples has confirmed the presence of NPs or NRs in the matrix of YBCO. Variation in the normal state resistivity and critical temperature in the resistivity versus temperature curve has been attributed to creation of the disorders, defects and inhomogeneity by the addition of NPs or NRs in the nanocomposite samples. The fluctuation-induced excess conductivity has been analyzed by using AL model which has shown the existence of five different fluctuation regimes near and above T_C . The decrement of 1D region width for NPs and increment for NRs have been attributed to the more destabilization of charge strips in NPs-added YBCO composite samples in comparison with NRs-added YBCO. A shift in the value of T_{LD} toward higher temperature with the increase in the concentration of NPs in composite samples has indicated the dominance of 3D regime, and a shift toward lower temperature values has indicated the dominance of the 2D regime with increasing concentration of NRs. The trend of d is similar to $\xi_C(0)$. A decrement in the value of $\xi_C(0)$ for 0.5 wt% added NPs or NRs-added YBCO sample in comparison with pure YBCO sample has been attributed to the increase in charge carrier density in the conducting planes. The enhancement in the superconducting parameters such as $B_{C1}(0)$, $B_{C2}(0)$ and $J_C(0)$ for the 0.5 wt% added NPs or NRs-added YBCO composite samples has been due to a reduction in magnetic vortex motion and enhancement in the pinning capability. NRs-added composite samples have shown more enhancement in $B_{C2}(0)$ and $J_C(0)$ in comparison with NPs-added samples which can be due to the presence of NRs in the matrix of YBCO inducing the creation of correlated defects which are acting as efficient APCs.

Acknowledgements All authors gratefully acknowledge the financial assistance from Ministry of Electronics and Information Technology (MeitY) and Department of Science and Technology, India, Project number RP03530 and MI01756. One of us (Mamta Dahiya) is thankful to the Council of Scientific and Industrial Research (CSIR), New Delhi, for providing Senior Research Fellowship (SRF) Grant (09/086(1273)/2017-EMR-I). The authors also acknowledge Nanoscale Research Facility (NRF) and Central Research Facility (CRF), IIT Delhi, for the use of XRD, FESEM, TEM and HRTEM facility.

Declarations

Conflict of interest The authors declare that they have no conflict of interest.

References

- J.R. Hull, Superconducting bearings. *Supercond. Sci. Technol.* **13**, R1–R15 (2000)
- J.H. Durrell, M.D. Ainslie, D. Zhou, P. Vanderbemden, T. Bradshaw, S. Speller, M. Filipenko, D.A. Cardwell, Bulk superconductors: a roadmap to applications. *Supercond. Sci. Technol.* **31**, 103501 (2018)
- K.B. Ma, Y.V. Postrekhin, W.K. Chu, Superconductor and magnet levitation devices. *Rev. Sci. Instrum.* **74**, 4989–5017 (2003)
- A.K. Jha, N. Khare, Investigation of flux pinning properties of YBCO:BaZrO₃ composite superconductor from temperature dependent magnetization studies. *J. Magn. Magn. Mater.* **322**, 2653–2657 (2010)
- B. Sahoo, K.L. Routray, B. Panda, D. Samal, D. Behera, Excess conductivity and magnetization of CoFe_2O_4 combined with $\text{Y}_1\text{Ba}_2\text{Cu}_3\text{O}_{7-\delta}$ as a superconductor. *J. Phys. Chem. Solids.* **132**, 187–196 (2019)
- W.K. Kwok, U. Welp, A. Glatz, A.E. Koshelev, K.J. Kihlstrom, G.W. Crabtree, Vortices in high-performance high-temperature superconductors. *Rep. Prog. Phys.* **79**, 116501 (2016)
- T.G. Holesinger, L. Civale, B. Maiorov, D.M. Feldmann, J.Y. Coulter, D.J. Miller, V.A. Maroni, Z. Chen, D.C. Larbalestier, R. Feenstra, X. Li, Y. Huang, T. Kodankandath, W. Zhang, M.W. Rupich, A.P. Malozemoff, Progress in nanoengineered microstructures for tunable high-current, high-temperature superconducting wires. *Adv. Mater.* **20**, 391–407 (2008)
- S. Nariki, N. Sakai, M. Murakami, I. Hirabayashi, Effect of $\text{RE}_2\text{BaCuO}_5$ refinement on the critical current density and trapped field of melt-textured (Gd, Y)–Ba–Cu–O bulk superconductors. *Physica C Supercond.* **439**, 62–66 (2006)
- G. Fuchs, K. Nenkov, G. Krabbes, R. Weinstein, A. Gandini, R. Sawh, B. Mayes, D. Parks, Strongly enhanced irreversibility fields and Bose-glass behaviour in bulk YBCO with discontinuous columnar irradiation defects. *Supercond. Sci. Technol.* **20**, 197 (2007)
- P.M.S. Raju, V. Seshubai, T. Rajasekharan, A generic process to introduce Nanoparticles into powder preforms and its application to Infiltration Growth processing of $\text{REBa}_2\text{Cu}_3\text{O}_7$ superconductor. *Mater. Chem. Phys.* **161**, 59–64 (2015)
- M.K.B. Salem, E. Hannachi, Y. Slimani, A. Hamrita, M. Zouaoui, L. Bessais, M.B. Salem, F.B. Azzouz, SiO_2 Nanoparticles addition effect on microstructure and pinning properties in $\text{YBa}_2\text{Cu}_3\text{O}_y$. *Ceram. Int.* **40**, 4953–4962 (2014)
- G. Hussain, A. Jabbar, I. Qasim, M. Mumtaz, K. Nadeem, M. Zubair, S.Q. Abbas, A.A. Khurram, Activation energy and excess conductivity analysis of $(\text{Ag})_x/\text{CuTi-1223}$ nano-superconductor composites. *J. Appl. Phys.* **116**, 103911 (2014)
- E. Hannachi, Y. Slimani, A. Ekicibil, A. Manikandan, F.B. Azzouz, Excess conductivity and AC susceptibility studies of Y-123 superconductor added with TiO_2 nano-wires. *Mater. Chem. Phys.* **235**, 121721 (2019)
- E. Hannachi, Y. Slimani, M.K.B. Salem, A. Hamrita, A.L. Al-Otaibi, M.A. Almessiere, M.B. Salem, F.B. Azzouz, Fluctuation induced conductivity studies in $\text{YBa}_2\text{Cu}_3\text{O}_y$ compound embedded by superconducting nano-particles Y-deficient $\text{YBa}_2\text{Cu}_3\text{O}_y$: effect of silver inclusion. *Indian J. Phys.* **90**, 1009–1018 (2016)
- A.L. Solovjov, V.M. Dmitriev, Fluctuation conductivity and pseudogap in high-temperature YBCO superconductors. *Fiz. Nizk. Temp.* **35**, 227–264 (2009)
- U.C. Upreti, A.V. Narlikar, Excess conductivity, critical region and anisotropy in $\text{YBa}_2\text{Cu}_4\text{O}_8$. *Solid State Commun.* **100**, 615–620 (1996)
- R. Hopfgärtner, B. Hensel, G. Saemann-Ischenko, Analysis of the fluctuation-induced excess dc conductivity of epitaxial

- YBa₂Cu₃O₇ films: influence of a short-wavelength cutoff in the fluctuation spectrum. *Phys. Rev. B*, **44**, 741–749 (1991)
18. A.A. Varlamov, The role of density of states fluctuations in the normal state anomalies of high T_C superconductors. *Phys. C Supercond. Appl.* **282–287**, 248–251 (1997)
 19. A.A. Varlamov, G. Balestrino, E. Milani, D.V. Livanov, The role of density of states fluctuations in the normal state properties of high T_C superconductors. *Adv. Phys.* **48**, 655–783 (1999)
 20. S.N. Bhatia, C.P. Dhard, Excess conductivity and pair-breaking effects in YBa₂Cu₃O₇ and Bi₂Sr₂Ca_{1-x}Y_xCu₂O₈₊ systems. *Phys. Rev. B*, **49**, 12206–12215 (1994)
 21. W.E. Lawrence, S. Doniach, Proc. 12th Int. Conf. Low Temp. Phys., Kyoto, Keigaku, Tokyo, (1970) 361
 22. L.G. Aslamasov, A.I. Larkin, The influence of fluctuation pairing of electrons on the conductivity of normal metal. *Phys. Lett. A*, **26**, 238–239 (1968)
 23. K. Maki, R.S. Thompson, Fluctuation conductivity of high-T_C superconductors. *Phys. Rev. B*, **39**, 2767–2770 (1989)
 24. M.A. Almessiere, E. Hannachi, Y. Slimani, G. Yasin, M. Mumtaz, M.R. Koblishka, A. Koblishka-Veneva, A. Manikandan, A. Baykal, Dimensionality and superconducting parameters of YBa₂Cu₃O_{7-d}/(WO₃ NP)_x composites deduced from excess conductivity analysis. *Mater. Chem. Phys.* **243**, 122665 (2020)
 25. Y. Slimani, Excess conductivity investigations of WO₃ nanowires added to YBa₂Cu₃O_{7-d} superconductor. *J. Mater. Sci. Mater. Electron.* **31**, 3023–3034 (2020)
 26. A.L. Al-Otaibi, M.A. Almessiere, M.B. Salem, F.B. Azzouz, Excess conductivity analysis in YBa₂Cu₃O_{7-d} added with SiO₂ nanoparticles and nanowires: comparative study. *Mod. Phys. Lett. B*, **30**, 1650242 (2016)
 27. W. Li, X. Xia, J. Zeng, L. Zheng, G. Li, Significant differences in NaNbO₃ ceramics fabricated using Nb₂O₅ precursors with various crystal structures. *Ceram. Int.* **46**, 3759–3766 (2020)
 28. D. Kumar, S. Singh, N. Khare, Plasmonic Ag nanoparticles decorated NaNbO₃ nanorods for efficient photoelectrochemical water splitting. *Int. J. Hydrogen Energy* **43**, 8198–8205 (2018)
 29. P.W. Anderson, Z. Zou, “Normal” tunneling and “Normal” transport: diagnostics for the resonating-valence-bond state. *Phys. Rev. Lett.* **60**, 132–135 (1988)
 30. A. Mellekh, M. Zouaoui, F.B. Azzouz, M. Annabi, M.B. Salem, Nano-Al₂O₃ particle addition effects on YBa₂Cu₃O_y superconducting properties. *Solid State Commun.* **140**, 318–323 (2006)
 31. D.K. Aswal, A. Singh, S. Sen, M. Kaur, C.S. Viswandham, G.L. Goswami, S.K. Gupta, Effect of grain boundaries on paraconductivity of YBa₂Cu₃O_x. *J. Phys. Chem. Solids.* **63**, 1797–1803 (2002)
 32. E.M.M. Ibrahim, S.A. Saleh, Influence of sintering temperature on excess conductivity in Bi-2223 superconductors. *Supercond. Sci. Technol.* **20**, 672–675 (2007)
 33. M. Sahoo, D. Behera, Effect of ferromagnetic induced inhomogeneity in excess conductivity of YBa₂Cu₃O_{7-x}+xCoFe₂O₄ composite. *J. Mater. Sci. Eng.* **01**, 1000115 (2012)
 34. Y. Slimani, E. Hannachi, M.K.B. Salem, A. Hamrita, M.B. Salem, F.B. Azzouz, Excess conductivity Study in nano-CoFe₂O₄-added YBa₂Cu₃O_{7-d} and Y₃Ba₅Cu₈O_{18+x} superconductors. *J. Supercond. Nov. Magn.* **28**, 3001–3010 (2015)
 35. M. Sahoo, D. Behera, Inhomogeneity induced conductivity fluctuation in YBa₂Cu₃O_{7-y}/Cr₂O₃ composite. *J. Supercond. Nov. Magn.* **26**, 3017–3025 (2013)
 36. A. Mohanta, D. Behera, Fluctuation induced magneto-conductivity studies in YBa₂Cu₃O_{7-δ} + xBaZrO₃ composite high-T_C superconductors. *Phys. C Supercond. Its Appl.* **470**, 295–303 (2010)
 37. X. Obradors, T. Puig, Coated conductors for power applications: materials challenges. *Supercond. Sci. Technol.* **27**, 044003 (2014)
 38. X. Obradors, T. Puig, S. Ricart, M. Coll, J. Gazquez, A. Palau, X. Granados, Growth, nanostructure and vortex pinning in superconducting YBa₂Cu₃O₇ thin films based on trifluoroacetate solutions. *Supercond. Sci. Technol.* **25**, 123001 (2012)

Publisher's Note Springer Nature remains neutral with regard to jurisdictional claims in published maps and institutional affiliations.